sensors

MDPI

Article

An Assessment of Anthropogenic CO_2 Emissions by Satellite-Based Observations in China

Shaoyuan Yang [1,2], Liping Lei [1,*], Zhaocheng Zeng [3], Zhonghua He [1,2] and Hui Zhong [1,2]

1 Key Laboratory of Digital Earth Science, Institute of Remote Sensing and Digital Earth, Chinese Academy of Sciences, Beijing 100094, China; yangsy@radi.ac.cn (S.Y.); hezhh@radi.ac.cn (Z.H.); zhonghui@radi.ac.cn (H.Z.)

2 University of Chinese Academy of Sciences, Beijing 100049, China

3 Division of Geological and Planetary Sciences, California Institute of Technology, Pasadena, CA 91125, USA; zzhaoch@gmail.com

* Correspondence: leilp@radi.ac.cn; Tel.: +86-010-82178162

Received: 2 January 2019; Accepted: 28 February 2019; Published: 5 March 2019

Abstract: Carbon dioxide (CO_2) is the most important anthropogenic greenhouse gas and its concentration in atmosphere has been increasing rapidly due to the increase of anthropogenic CO_2 emissions. Quantifying anthropogenic CO_2 emissions is essential to evaluate the measures for mitigating climate change. Satellite-based measurements of greenhouse gases greatly advance the way of monitoring atmospheric CO_2 concentration. In this study, we propose an approach for estimating anthropogenic CO_2 emissions by an artificial neural network using column-average dry air mole fraction of CO_2 (XCO_2) derived from observations of Greenhouse gases Observing SATellite (GOSAT) in China. First, we use annual XCO_2 anomalies ($dXCO_2$) derived from XCO_2 and anthropogenic emission data during 2010–2014 as the training dataset to build a General Regression Neural Network (GRNN) model. Second, applying the built model to annual $dXCO_2$ in 2015, we estimate the corresponding emission and verify them using ODIAC emission. As a results, the estimated emissions significantly demonstrate positive correlation with that of ODIAC CO_2 emissions especially in the areas with high anthropogenic CO_2 emissions. Our results indicate that XCO_2 data from satellite observations can be applied in estimating anthropogenic CO_2 emissions at regional scale by the machine learning. This developed method can estimate carbon emission inventory in a data-driven way. In particular, it is expected that the estimation accuracy can be further improved when combined with other data sources, related CO_2 uptake and emissions, from satellite observations.

Keywords: anthropogenic CO_2 emissions; GOSAT; atmospheric CO_2 concentration

1. Introduction

Atmospheric carbon dioxide (CO_2) is the most significant anthropogenic greenhouse gas (GHG) and its concentration in atmosphere has been increasing from 280 ppm since the preindustrial era to a level higher than 400 ppm at present at a global scale [1]. The enhancement of atmospheric CO_2 has been known as one of the factors inducing global warming and playing an important role in climate change. Anthropogenic CO_2 emissions, 70% of which come from fossil fuel combustion and industrial activities [2], are the main driver of the atmospheric CO_2 concentration increase. If atmospheric CO_2 concentration continues to increase at the current rate, 1.5 °C of global warming will be reached between 2030 and 2052, which will cause more climate extremes [3]. Atmospheric CO_2 concentration, moreover, will be continually increasing as the rapid development of industrialization requires enormous energy around the world. In order to slow down the increase of atmospheric CO_2

concentration, many countries are making efforts for CO_2 emissions reduction. For that we need an efficient and reliable way to monitor CO_2 emissions in order to evaluate the effectiveness of CO_2 emissions reduction policy.

Over the past 20 years, satellite-based measurements of greenhouse gases have been facilitating the way monitoring atmospheric constituents with the great advancement of satellite observing technology in the development of highly accurate sensors. It is also becoming the major data source to detect the change of atmospheric CO_2 concentration at regional and global scales [4–7]. Compared with ground-based observation, CO_2 concentration retrieved by satellite has global coverage and consistent observation characteristics, which can better reveal the spatio-temporal variation of atmospheric CO_2 concentration. Currently, the GHG observing satellites in orbit include the Greenhouse gases Observing SATellite (GOSAT) from Japan, Orbiting Carbon Observatory 2 (OCO-2) from the USA and TanSat from China, which can provide us the column-averaged dry air mole fraction of CO_2 (XCO_2) dataset since 2009 [8–10].

Many previous studies indicated that XCO_2 retrieved from satellite observations can detect changes of CO_2 concentration induced by anthropogenic emissions [11–13]. The anthropogenic emission is expected to induce an increase of about 4 ppm of XCO_2 around power plants [11]. With multi-year XCO_2 dataset available from GOSAT and OCO-2, anthropogenic CO_2 emissions have been quantified by excluding the background concentration. It was reported that megacities such as Los Angeles and Beijing, and high density urban regions such as eastern USA and the Beijing-Tianjin-Hebei area in northern China have about 2 ppm enhancements [14–16]. These studies mainly obtained regional CO_2 enhancements in contrast to the background using empirical conversion factors. It has been shown that the XCO_2 has a positive correlation with the anthropogenic CO_2 emissions through correlating OCO-2 observations with emission inventories [17]. The correlation implies that satellite-based observations are capable to quantitatively assess the anthropogenic CO_2 emissions through detection of XCO_2 enhancements. Estimation of anthropogenic emissions from satellite-based observation can support the investigation of carbon emissions as a data-driven method, which is different to the conventional method in calculating emission inventory. Satellite observations can detect the CO_2 changes in specific regions such as strong sources of anthropogenic emissions, e.g., megacities and high density urban area, so as to monitor CO_2 emissions effectively. These studies, however, mostly focus on investigating enhancement of CO_2 induced by anthropogenic emissions through regional contrast. It is still a challenge in using XCO_2 data to quantitatively estimate the magnitude of anthropogenic CO_2 emissions. This data-driven approach, as an additional way of quantifying anthropogenic CO_2 emissions, can help policymakers to obtain more information for evaluating the effects for CO_2 emissions reduction at both regional and global scales.

In this paper, we propose a method of using satellite-based observation to assess the anthropogenic CO_2 emissions aiming to assist the national routine investigation of carbon emissions. We focus on mainland China as the studying area since it is a major national emitter of CO_2 [18]. We extracted XCO_2 anomalies ($dXCO_2$) using XCO_2 dataset obtained from GOSAT observations. The anomalies are found to be significantly correlated with anthropogenic CO_2 emissions from the CO_2 emitting sources such as power plant emission. We further introduce artificial neural network algorithm (ANN) to construct an estimation model for anthropogenic CO_2 emissions based on the changes of atmospheric CO_2 concentration derived from satellite observations.

2. Data and Methodology

2.1. XCO_2 Retrievals and Mapping XCO_2 Dataset

XCO_2 retrieval data products from January 2010 to December 2015 are collected from GOSAT Atmospheric CO_2 Observations from Space (ACOS v7.3). This dataset was produced by the Orbiting Carbon Observatory (OCO) team of the US National Aeronautics and Space Administration (NASA) using a full physics algorithm to retrieve XCO_2 from GOSAT's Spectrometer (TANSO-FTS) calibrated

spectra measurements (Level 1B) [19]. In order to ensure high reliability of the data, only those data over land with high gain are used after screening and correction of systematic bias as described in the ACOS Level 2 Standard Product and Lite Data Product Data User's Guide, v7.3 [20]. ACOS XCO_2 retrievals have a standard deviation of error of 1.48 ppm when comparing with ground-based measures of Total Carbon Column Observing Network (TCCON) [21]. Figure 1 shows the total counts of XCO_2 data points during 6 years from January 2010 to December 2015, and their temporal variation in the study area. An annual increase of XCO_2 and the seasonal variation can be clearly seen.

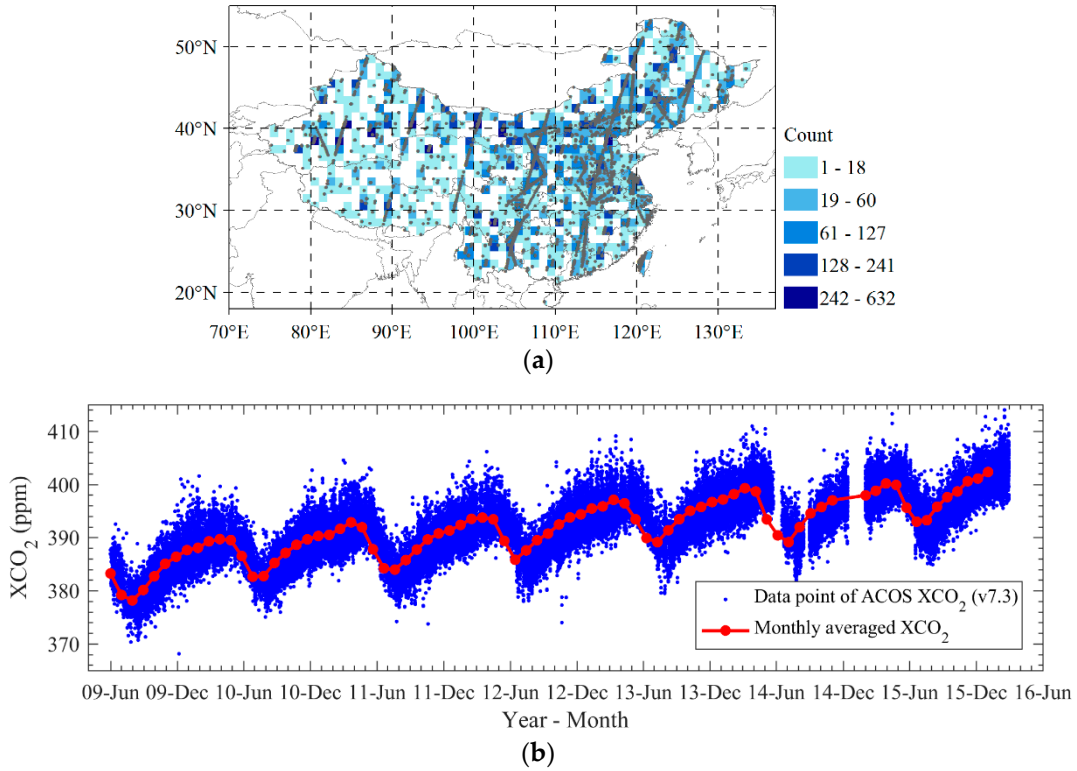

Figure 1. Number of available retrievals and temporal changes of collected XCO_2 data: (**a**) the number of XCO_2 data points within 1° × 1° grid for 6 years from 2010 to 2015; (**b**) the temporal variation of XCO_2 and the monthly averages.

However, XCO_2 data are irregularly distributed and have many gaps in space and time as shown in Figure 1a because of the limitation of GOSAT observation mode, cloudy and data screening. To investigate the space-time changes of XCO_2, we generate a mapping XCO_2 dataset in which those gaps are filled using the kriging interpolation method based on the spatio-temporal geo-statistics model [22–24]. The mapping XCO_2 dataset is generated mainly in Chinese mainland area from 18° N to 57° N and from 65° E to 148° E with 0.5° × 0.5° grid cells and 3-day interval in time from 1 January 2010 to 31 December 2015. In order to match with collected ODIAC emission dataset in 1° × 1°, we resampled the spatial resolution of data we used in this paper to 1° × 1°. This mapping dataset is hereafter referred to as Mapping-XCO_2.

2.2. Anthropogenic Emission Data

We collected two datasets of the bottom-up anthropogenic CO_2 emissions. One is the Open-source Data Inventory for Anthropogenic Carbon dioxide (ODIAC) for same years as the used XCO_2 dataset in this study. The other is the CARbon Monitoring for Action (CARMA) power plant database in 2009. The specifications of these data are described in Table 1.

Table 1. Basic specifications of ODIAC and CARMA bottom-up CO_2 emission datasets.

	ODIAC	CARMA
Grid, timely unit/period	1° × 1°, Month/2010–2015	Points/2009
Unit	Ton	Ton
Statistical sectors	Point sources non-point sources	-
	Cement production	
	Gas flaring	
	International aviation and marine bunker	
Used data sources	Fuel statistic data published as united nation energy statistics database BP statistical review of world energy 2017	The environmental protection agency and department of energy International atomic energy agency
Producer	Center for global environment research, national institute for environment studies	Center for Global Development
	Oda, T et al. [25]	Wheeler, D et al. [26]

The ODIAC emissions data product is a global 1° × 1° gridded monthly fossil fuel CO_2 emission inventory, developed based on country level fossil fuel CO_2 emission estimates, fuel consumption statistics, satellite-observed nightlight data, and point source information (geographical locations and emission intensities) from the CARbon Monitoring for Action (CARMA) power plant database (ODIAC2015a, available at http://db.cger.nies.go.jp/dataset/ODIAC/). The global nightlight data were used as a geo-referenced, spatial proxy to determine the spatial extent of anthropogenic emissions from line and diffused (area) sources (e.g., road traffic, residential or commercial fuel consumption) [25]. The ODIAC gridded emissions fields defined on a global rectangular (latitude ×longitude) coordinate are remapped to meet the grids resolutions for each simulation domain.

Additionally, the CO2 emissions from power plant, which is one of the dominant CO_2 emitting sources, are collected in the study area from the database of Carbon Monitoring for Action (CARMA, available at http://carma.org/plant). At the same time, we unify the units of the two sets of emission data to ton, and take the logarithm of two emission data base on 10 (refer to as lgE) to facilitate the calculation.

2.3. Methodology

The method for estimating anthropogenic CO_2 emission include three major steps as shown in Figure 2.

Firstly, we enhance the signals of CO_2 from anthropogenic emission in XCO_2 which is described in Section 2.3.1. Secondly, we apply the training datasets of XCO_2 and ODIAC in 2010–2014 to GRNN to get the estimating model of anthropogenic emission which is described in Section 2.3.2 in detail. Thirdly, anthropogenic emissions are estimated by GRNN model using XCO_2 in 2015, and validated by comparing with ODIAC data in 2015.

2.3.1. Variable of XCO_2 Used for Estimation of Anthropogenic Emission

The magnitude of XCO_2 include CO_2 emitted by anthropogenic activities, the fluxes of terrestrial biosphere, fluxes transported by atmospheric wind fields [27,28] and CO_2 of regional background. We introduce therefrom an interannual variability by removing the regional background signal and calculating their annual mean to enhance the signals of CO_2 from anthropogenic emission as following equation proposed by Hakkarainen et al. [17]:

$$dXCO_2(grid, t) = XCO_2(grid, t) - MXCO_2(t) \quad (1)$$

where $dXCO_2$ (grid,t) indicates the deviation from regional background for each grid at a specific time unit t where t is the 3-day unit of used mapping-XCO_2 data; XCO_2 (grid,t) is XCO_2 for each grid at time t from mapping-XCO_2 data; $MXCO_2$(t) is median of XCO_2 for all girds in the study region at time

t calculated from mapping-XCO_2 data with 0.5° × 0.5° grid cell. Lastly we apply the annual mean of $dXCO_2$ (grid,t) for the year from 2010 to 2015 in the estimation of anthropogenic emission. This annual mean of $dXCO_2$ (grid,t) could detrend the seasonal variation at locale and simultaneously reduces the effect of the atmospheric transport [17].

We computed the monthly averaged $dXCO_2$ and annual averaged $dXCO_2$ for each grid to generate monthly averaged $dXCO_2$ dataset and annual averaged $dXCO_2$ dataset from the year 2010 to 2015 with 1° × 1° grids using the mapping XCO_2 dataset from 2010 to 2015. The annual $dXCO_2$ dataset and ODIAC data will be used in the following analysis.

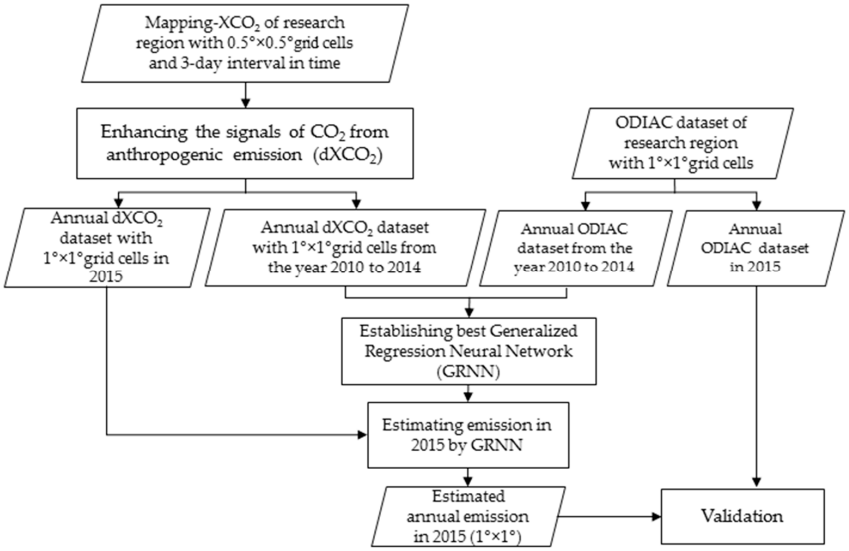

Figure 2. Flowchart of estimating anthropogenic emission using XCO_2 data obtained by GOSAT observations. It consists of three major steps, firstly enhancing the signals of CO_2 from anthropogenic emission in XCO_2; secondly establishing GRNN model using the training datasets; the last estimating the anthropogenic emissions and validating the result.

2.3.2. Estimation of Anthropogenic CO_2 Emission by Neural Network Development

Because XCO_2 variations are forced by anthropogenic emissions, exchange between the atmosphere and the ocean and the terrestrial biosphere [27,28], there are both non-linear and linear mapping between XCO_2 and emissions. Here we adopt a General Regression Neural Network (GRNN) algorithm [29] to represent non-linear mapping between the independent variables ($dXCO_2$ in this study) and dependent variable (CO_2 emissions in this study). GRNN directly draws the function estimate approximating any arbitrary function between the input and output vectors of variables. The GRNN converges to the optimal regression result when the training samples increases in number, meanwhile, the error of estimation is closed to 0. There are four layers in the GRNN model we used, an input layer, a hidden layer, a summation layer, and a decision layer (Figure 3; [30,31]). In the input layer, each neuron corresponds to an independent variable which is defined as a mathematical function, the independent variable values will be standardized. Then the standardized independent variable values were transferred to the neurons in the hidden layer. In this layer, each neurons stores the values of the independent variables and the dependent variable, and a scalar function will be calculated. There are two neurons in the summation layer, the denominator summation unit sums the weight values coming from the hidden neurons, and the numerator summation unit sums the weight values multiplied by the actual target dependent variable value for each hidden neuron. At last, dividing the value accumulated in the numerator summation unit by the value in the denominator summation unit in the decision layer, we uses the division result as the predicted target dependent variable value [32].

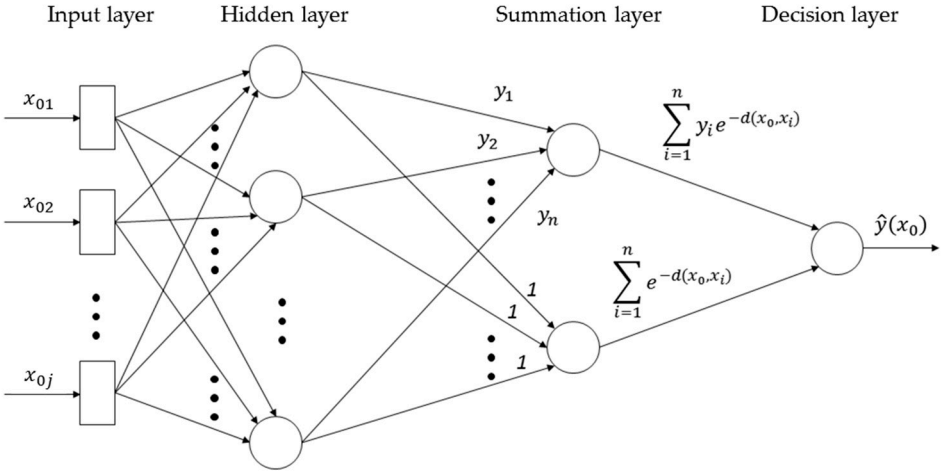

Figure 3. Schematic diagram of the generalized regression neural network architecture based on Cigizolu and Alp [30].

According to the calculation steps of developing a neural network, we need to standardize all the independent and dependent training variables, so that in the input layer all training data will have the same order of magnitudes.

$$d(x_0 - x_i) = \sum_{j=1}^{p} \left[\frac{x_{0j} - x_{ij}}{\sigma} \right]^2 \quad (2)$$

where p denotes the dimension of variable vector x_i, σ is the spread parameter, whose optimal value is determined by minimizing the root mean square error (RMSE) between the training data and the predicted values of the dependent variable.

The weight of the denominator neuron is set to 1.0. The GRNN training algorithm uses only one adjustable parameter σ for a given training set. Here we use "the holdout method" [29] to optimize the σ value, and detailed introduction can refer to the article [29]. The predicted target dependent variable, the ODIAC CO_2 emissions, is defined by the following Equation (3):

$$\hat{y}(x_0) = \frac{\sum_{i=1}^{n} y_i e^{-d(x_0,x_i)}}{\sum_{i=1}^{n} e^{-d(x_0,x_i)}} \quad (3)$$

where the values calculated with the scalar function in a hidden neuron i are weighted with the corresponding values of the training samples y_i, and then passed to the numerator neuron. n is the number of training samples.

3. Results and Discussion

3.1. Estimated Anthropogenic Emissions by GRNN

We use the annual $dXCO_2$ dataset and ODIAC CO_2 emissions data from the year 2010 to 2014 as the training dataset, which have the total of 5415 samples available, to build a GRNN model for estimating anthropogenic emission. By applying "the holdout method" described in Section 2.3, we obtain the optimized spread parameter σ as 0.1. Then we apply GRNN model to the annual $dXCO_2$ data in 2015 to predict target dependent variable, anthropogenic emission with the same unit as the ODIAC CO_2 emissions.

The CO_2 emissions estimated using the annual $dXCO_2$ and the actual ODIAC CO_2 emission in 2015 are shown in Figure 4. Comparing Figure 4a with Figure 4b, we can see that the spatially changing pattern of estimated emission by satellite-based observation is exactly similar as that of the actual magnitude of ODIAC. Moreover, the estimated emission presents a more smoothing spatial details than the actual emission, which is mainly because the Kriging procedure smooths the CO_2 signals

from point sources of strong anthropogenic emission, and 10 km spatial resolution of each GOSAT footprint observations also smooths the signals. The magnitude of estimated emission is generally less than that of ODIAC. Figure 5 presents the differences between them and the corresponding histogram.

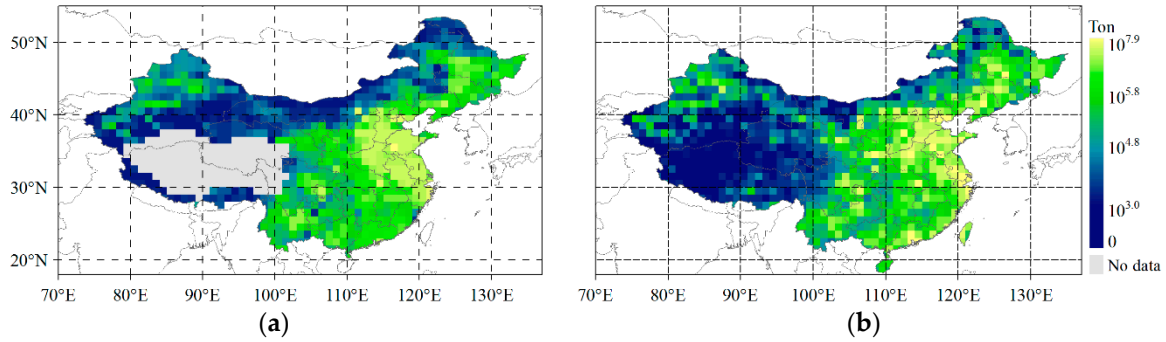

Figure 4. The anthropogenic CO_2 emissions in 2015 in China: (**a**) CO_2 emission estimated using GRNN based on the annual $dXCO_2$ in 2015 from GOSAT observations. The Tibet area shown as blank is filtered due to their high uncertainty XCO_2 retrievals; (**b**) the CO2 emission from ODIAC in 2015.

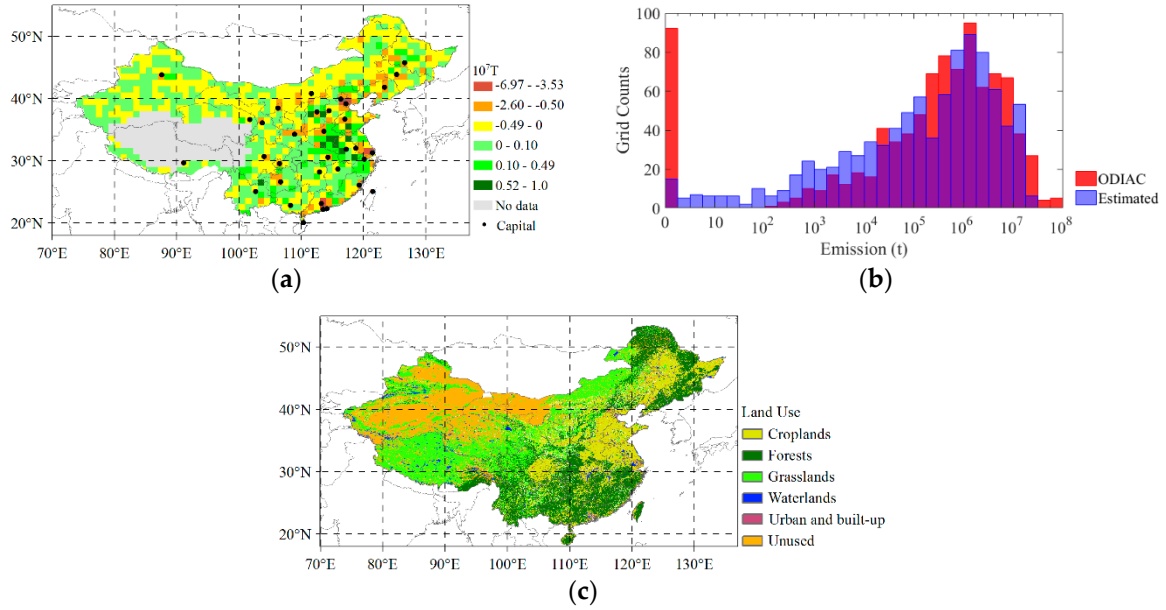

Figure 5. (**a**) The difference between the estimated CO_2 emission using mapping-XCO_2 in 2015 and ODIAC emission in 2015; (**b**) Histogram comparison of the estimated and the ODIAC CO_2 emission (in unit of Ton/year) in 2015; (**c**) Land use of China in 2010.

It can be seen from Figure 5a that the difference between the estimated CO_2 emission and ODIAC emission mainly change from −5 Mt to 5 Mt, which accounts for 91% of the total grids. The magnitude of difference from −1 Mt to 1 Mt accounts for 71% of the total grids. The low magnitude of ODIAC emissions in the range of 1–10^4 t/year shown in Figure 4b are generally underestimated by satellite-based observations (shown in yellow in Figure 5a). These are mostly located in semi-arid grasslands, forests in the northern areas as shown in land use map of Figure 5c.

This underestimation implies that the emission estimated by $dXCO_2$ has high uncertainty in the areas of low anthropogenic emission that is likely due to the CO_2 uptake of biosphere which is still remaining in $dXCO_2$. The estimated emission, moreover, is much lower than ODIAC emission over the areas around big cities, such as Beijing, Shanghai, Guangzhou. This underestimation indicates that the smoothing effects of the estimated emission, which is likely because the spatial resolution of GOSAT observations (10 km) is not sufficient to detect the emission of point sources. On the other

hand, the estimated emissions are generally larger than ODIAC emission in the south-eastern region of China where there are many anthropogenic emitting sources which can be seen in Figure 8. The general overestimation in this region is likely because the large emitting sources around raise the concentration of CO_2 over those non-emitting areas nearby them through the atmospheric transport.

Lastly, comparing the satellite-based estimation of CO_2 emissions with ODIAC emission for all grids as shown in Figure 6, we find they show a significant correlation (R^2) of 0.65 with p value less than 0.01.

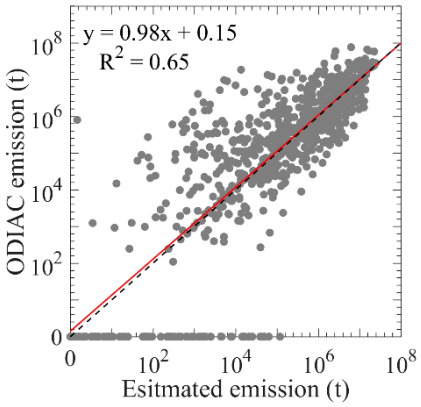

Figure 6. Scatterplot between estimated CO_2 emission using mapped-XCO_2 data and the actual ODIAC emission in 2015, in which red line is the regression line between estimated emission and ODIAC emission, and black dotted line is the 1:1 line.

3.2. Discussion of Correlation between Retrieved X_{CO2} and Anthropogenic Emissons

It has been indicated that the cluster of XCO_2 changes derived from GOSAT observations shows a correlating coefficient of 0.5 with anthropogenic emission. This correlation is more significant than a single grid of XCO_2 as the atmospheric CO_2 measurement is an instantaneous snapshot of the realistic atmosphere [33]. Its clustering analysis is derived from original XCO_2 data.

We segment the ODIAC emissions which are binned according to every 0.3 t/yr of lgE (Figure 7a) using mean emission calculated from annual emission during 2010–2015, and then make correlation analysis between the mean of emission and mean of $dXCO_2$ within binned regions. It is found that the segmental mean of $dXCO_2$ demonstrate a significant and positive correlation with ODIAC emissions in which the determined coefficient (R^2) for all data is up to 0.82 (Figure 7b) and the $dXCO_2$ demonstrate strong positive linear correlation with emission starting from 10^4 t/yr where R^2 is up to 0.95 (red line in Figure 7b). The $dXCO_2$ is almost unchanged in the region with emission lower than 10^4 t/yr. These results imply that satellite observations of atmospheric CO_2 could be used to estimate regional anthropogenic emissions for those regions with larger magnitude of anthropogenic CO_2 emissions. Additionally, we overlay the CARMA power plants dataset on the mean $dXCO_2$ from the annual $dXCO_2$ during 2010 to 2015 (Figure 8a). It can be seen that the high $dXCO_2$ are corresponding to high-density power plants, especially in northeast China. We accumulate the magnitude of emissions of power plants within one grid of mapping XCO_2 dataset, then we segment emissions of power plants which are binned according to every 0.3 t of lgE, and take correlation analysis between the mean of power plants emission and the mean of $dXCO_2$ within binned regions (Figure 8a). $dXCO_2$ demonstrate strong positive linear correlation with power plants emission starting from 10^6 t (blue dots). The grids they represent are distributed consistently with high $dXCO_2$ area. The result demonstrates a R^2 of 0.59 which is less than regional statistics. Power plants emission lower than $10^{5.5}$ t demonstrate weak linear correlation with $dXCO_2$ because the influence of CO_2 uptake of biosphere.

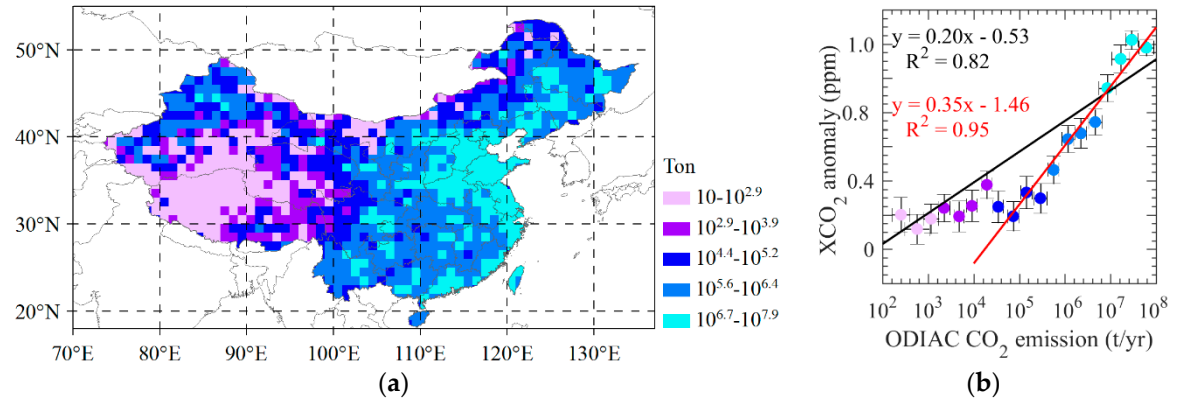

Figure 7. (**a**) Segment of ODIAC emissions, where the data are binned by every 0.3 t/yr of lgE using mean emission calculated from annual emission during 2010–2015; (**b**) correlation between mean ODIAC CO_2 emissions and mean $dXCO_2$ calculated from annual $dXCO_2$ during 2010–2015 for each segment, where red line is the regression line between $dXCO_2$ and ODIAC CO_2 emissions with emission lager than 10^4 t/yr.

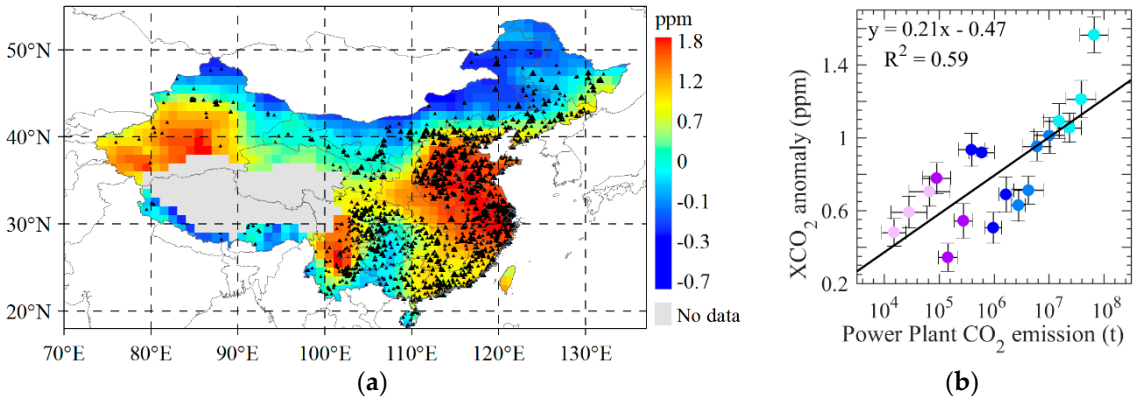

Figure 8. (**a**) the mean of $dXCO_2$ from the annual $dXCO_2$ during 2010 to 2015 overlaid with CARMA power plants locations; (**b**) the correlation between emission of CARMA power plants within 1° × 1° grid which are binned by every 0.3 t/yr of lgE and the corresponding mean $dXCO_2$, different color dots represent different segment of CARMA power plants emissions.

From Figure 8a, it can be found that the $dXCO_2$ in western area, the desert area of Xinjiang, shows high values even if there are much less anthropogenic emission over this area as shown in Figure 4b. This is likely resulted in the uncertainty of ACOS XCO_2 retrievals in desert which has been indicated by Bie et al. [34].

4. Conclusions

In this paper, to support the verification of bottom-up inventory of anthropogenic emission, an anthropogenic CO_2 emission estimation method using a machine learning technique is applied to the gap-filled ACOS XCO_2 dataset over the mainland of China derived from GOSAT observations. The annual emission signatures, indicated by $dXCO_2$, is enhanced by removing the background XCO_2 from the 2010 to 2015 XCO_2 data. We then apply the annual averaged $dXCO_2$ from 2010 to 2014 to build an estimating model of anthropogenic emission using an artificial network approach. The model is verified by estimating results in 2015 and comparing with the ODIAC emissions. Lastly, we quantify the correlation between the annual $dXCO_2$ and the magnitude of anthropogenic emission. Our result indicate that the anthropogenic emission can be estimated at regional scale by the changing magnitude of XCO_2 especially for those regions with larger emissions. However, it has relatively higher uncertainty to grasp the CO_2 signals of the low or without anthropogenic emission areas and

point emitting sources. The CO_2 uptake of biosphere and fluxes of wind field affect the estimation when using the annual $dXCO_2$. The observation mode of GOSAT satellite in space and time and fast mixing of atmospheric CO_2 also affect the detection of point emitting sources.

Our study demonstrates that the XCO_2 derived from satellite observation can effectively provide a way to reveal the spatial patterns of underlying anthropogenic emissions. It is expected that the estimation of anthropogenic emission could be greatly improved by using more and more XCO_2 data from multi-satellite such as OCO-2, OCO-3, GOSAT-2, and TanSat in future. Moreover, we can combine the ancillary data related with CO_2 uptake and emission which can be obtained by satellite remote sensing observations at the same time, such as gross primary production (GPP), industrial heat source from VIIRS (Visible infrared Imaging Radiometer) Night fire product for point sources, Night light from Defense Meteorological Satellite Program/Operational Linescan System (DMSP/OLS), to constrain the estimating model developed in this study. This data-driven approach based on satellite-based observations can offer the possibility of rapid updates for anthropogenic CO_2 emissions, and provide a new way of investigating anthropogenic emissions to support the implement of regional reduction of carbon emissions.

Author Contributions: S.Y. and L.L. conceived and designed the experiments; S.Y. performed the experiments; S.Y. and L.L. analyzed the data; Z.Z., Z.H. and Z.H. contributed analysis tools; S.Y. and L.L. wrote the paper. All authors proofread the manuscript.

Funding: This research were funded by Key Program of the Chinese Academy of Sciences (Grand No.ZDRW-ZS-2019-1) and CAS Earth Big Data Science Project: "Global Medium and Low Resolution Time Series Spatial Information Products" (Grant No.XDA19080303). And the APC was funded by Key Program of the Chinese Academy of Sciences.

Acknowledgments: We acknowledge The ACOS-GOSAT v7.3 data were produced from the ACOS/OCO-2 project at the Jet Propulsion Laboratory, California Institute of Technology, and obtained from the ACOS/OCO-2 data archive maintained at the NASA Goddard Earth Science Data and Information Services Center. We also acknowledge the Center for Global Environmental Research, National Institute for Environmental Studies for providing ODIAC2015a dataset at http://db.cger.nies.go.jp/dataset/ODIAC/. CARMA are provided by the Center for Global Development, Washington, DC. The dataset was available at http://carma.org/plant.

Conflicts of Interest: The authors declare no conflict of interest.

References

1. World Meteorological Organization (WMO). Greenhouse Gas Bulletin, No. 13. Available online: https://public.wmo.int/en/media/press-release/greenhouse-gas-concentrations-surge-new-record (accessed on 2 January 2019).
2. IPCC. Summary for Policymakers. In *Climate Change 2013: The Physical Science Basis*; Contribution of Working Group I to the Fifth Assessment Report of the Intergovernmental Panel on Climate Change; Stocker, T.F., Qin, D., Plattner, G.-K., Tignor, M., Allen, S.K., Boschung, J., Nauels, A., Xia, Y., Bex, V., Midgley, P.M., Eds.; Cambridge University Press: Cambridge, UK; New York, NY, USA, 2013; Volume 3, pp. 3–29.
3. IPCC. Summary for Policymakers. In *Global Warming of 1.5 °C*; An IPCC Special Report on the Impacts of Global Warming of 1.5 °C above Pre-Industrial Levels and Related Global Greenhouse Gas Emission Pathways, in the Context of Strengthening the Global Response to the Threat of Climate Change, Sustainable Development, and Efforts to Eradicate Poverty; Masson-Delmotte, V., Zhai, P., Pörtner, H.-O., Roberts, D., Skea, J., Shukla, P.R., Pirani, A., Moufouma-Okia, W., Péan, C., Pidcock, R., et al., Eds.; World Meteorological Organization: Geneva, Switzerland, 2018; pp. 6–13.
4. Yoshida, Y.; Ota, Y.; Eguchi, N.; Kikuchi, N.; Nobuta, K.; Tran, H.; Morino, I.; Yokota, T. Retrieval algorithm for CO_2 and CH_4 column abundances from short-wavelength infrared spectral observations by the greenhouse gases observing satellite. *Atmos. Meas. Tech.* **2011**, *4*, 717–734. [CrossRef]
5. Crisp, D.; Miller, C.; Team, O.S. Contributions of the Orbiting Carbon Observatory (OCO) to the detection of anthropogenic CO_2 emissions. *ADS Abstr. Serv.* **2015**, *19*, 73–86.
6. Lei, L.P.; Guan, X.H.; Zeng, Z.Z.; Zhang, B.; Ru, F.; Bu, R. A comparison of atmospheric CO_2 concentration GOSAT-based observations and model simulations. *Sci. China Earth Sci.* **2014**, *57*, 1393–1402. [CrossRef]

7. Buchwitz, M.; Reuter, M.; Schnesing, O.; Boesch, H.; Guerlet, S.; Dils, B.; Aben, I.; Armante, R.; Bergamaschi, P.; Bovensmann, H.; et al. The Greenhouse Gas Climate Change Initiative (GHG-CCI): Comparison and quality assessment of near-surface-sensitive satellite-derived CO_2 and CH_4 global data sets. *Remote Sens. Environ.* **2015**, *162*, 344–362. [CrossRef]
8. Crisp, D.; Miller, C.E.; DeCola, P.L. NASA Orbiting Carbon Observatory: Measuring the column averaged carbon dioxide mole fraction from space. *J. Appl. Remote Sens.* **2008**, *2*, 142–154. [CrossRef]
9. Yoshida, T.; Yoshida, Y.; Eguchi, N.; Ota, Y.; Tanaka, T.; Watanabe, H.; Maksyutov, S. Global concentrations of CO_2 and CH_4 retrieved from GOSAT: First preliminary results. *Sci. Online Lett. Atmos. Sola* **2009**, *5*, 160–163.
10. Liu, Y.; Yang, D.X.; Cai, Z.N. A retrieval algorithm for TanSat XCO_2 observation: Retrieval experiments using GOSAT data. *Chin. Sci. Bull.* **2013**, *58*, 1520–1523. [CrossRef]
11. Bovensmann, H.; Buchwitz, M.; Burrows, J.P.; Reuter, M.; Krings, T.; Gerilowski, K.; Schneising, O.; Heymann, J.; Tretner, A.; Erzinger, J. A remote sensing technique for global monitoring of power plant CO_2 emissions from space and related applications. *Atmos. Meas. Tech.* **2010**, *3*, 781–811. [CrossRef]
12. Schneising, O.; Heymann, J.; Buchwitz, M.; Reuter, M.; Bovensmann, H.; Burrows, J. Anthropogenic carbon dioxide source areas observed from space: Assessment of regional enhancements and trends. *Atmos. Chem. Phys.* **2013**, *13*, 2445–2454. [CrossRef]
13. Keppel-Aleks, G.; Wennberg, P.O.; O'Dell, C.W.; Wunch, D. Towards constraints on fossil fuel emissions from total column carbon dioxide. *Atmos. Chem. Phys.* **2013**, *13*, 4349–4357. [CrossRef]
14. Kort, E.A.; Frankenberg, C.; Miller, C.; Oda, T. Space-based observations of megacity carbon dioxide. *Geophys. Res. Lett.* **2012**, *39*, L17806. [CrossRef]
15. Janardanan, R.; Maksyutov, S.; Oda, T.; Saito, M.; Kaiser, J.W.; Ganshin, A.; Stohl, A.; Matsunaga, T.; Yoshida, Y.; Yokota, T. Comparing GOSAT observations of localized CO_2 enhancements by large emitters with inventory-based estimates. *Geophys. Res. Lett.* **2016**, *43*, 3486–3493. [CrossRef]
16. Lei, L.P.; Zhong, H.; He, Z.H.; Cai, B.F.; Yang, S.Y.; Wu, C.J.; Zeng, Z.C.; Liu, L.Y.; Zhang, B. Assessment of atmospheric CO2 concentration enhancement from anthropogenic emissions based on satellite observations. *Chin. Sci. Bull.* **2017**, *25*, 2941–2950. [CrossRef]
17. Hakkarainen, J.; Ialongo, I.; Tamminen, J. Direct space-based observations of anthropogenic CO_2 emission areas from OCO-2. *Geophys. Res. Lett.* **2016**, *43*, 400–411. [CrossRef]
18. International Energy Agency (IEA). CO_2 Emissions from Fuel Combustion Overview (2018 Edition). Available online: https://webstore.iea.org/co2-emissions-from-fuel-combustion-2018 (accessed on 2 January 2019).
19. O'Dell, C.W.; Connor, B.; Bösch, H.; Brien, D.; Frankenberg, C.; Castano, R.; Christi, M.; Eldering, D.; Fisher, B.; Gunson, M.; et al. The ACOS CO_2 retrieval algorithm—Part 1: Description and validation against synthetic observations. *Atmos. Meas. Tech.* **2012**, *5*, 99–121.
20. Osterman, G.; Eldering, A.; Cheng, C.; O'Dell, C.W.; Crisp, D. *Christian Frankenberg. Brendan Fisher. ACOS Level 2 Standard Product and Lite Data Product Data User's Guide, v7.3*; NASA GES DISC: Pasadena, CA, USA, 2017.
21. Wunch, D.; Toon, G.C.; Blavier, J.F.L.; Washenfelder, R.A.; Notholt, J.; Connor, B.J.; Griffith, D.W.T.; Sherlock, V.; Wennberg, P.O. The total carbon column observing network. *Philos. Trans. R. Soc. Lond. A Math. Phys. Eng. Sci.* **2011**, *369*, 2087–2112. [CrossRef] [PubMed]
22. Zeng, Z.C.; Lei, L.P.; Guo, L.J.; Zhang, L.; Zhang, B. Incorporating temporal variability to improve geostatistical analysis of satellite-observed CO_2 in China. *Chin. Sci. Bull.* **2013**, *58*, 1948–1954. [CrossRef]
23. Zeng, Z.C.; Lei, L.P.; Hou, S.S.; Ru, F.; Guan, X.X.; Zhang, B. A Regional Gap-Filling Method Based on Spatiotemporal Variogram Model of CO_2 Columns. *IEEE Transaftions Geosci. Remote Sens.* **2014**, *52*, 3594–3603. [CrossRef]
24. Guo, L.J.; Lei, L.P.; Zeng, Z.C.; Zou, P.F.; Liu, D.; Zhang, B. Evaluation of Spatio-Temporal Variogram Models for Mapping XCO_2 Using Satellite Observations: A Case Study in China. *IEEE J. Sel. Top. Appl. Earth Obs. Remote Sens.* **2015**, *8*, 376–385. [CrossRef]
25. Oda, T.; Maksyutov, S.; Andres, R.J. The Open-source Data Inventory for Anthropogenic Carbon dioxide (CO_2), version 2016 (ODIAC2016): A global, monthly fossil-fuel CO_2 gridded emission data product for tracer transport simulations and surface flux inversions. *Earth Syst. Sci. Data* **2018**, *10*, 87–107. [CrossRef]
26. Wheelwer, D.; Ummel, K. *Calculating CARMA: Global Estimation of CO2 Emissions from the Power Sector*; Working Papers; Center for Global Development: Washington, DC, USA, 2008.

27. Suntharalingam, P.; Jacob, D.J.; Palmer, P.I.; Logan, J.A.; Yantosca, R.M.; Xiao, Y.P.; Evans, M.J. Improved quantification of Chinese carbon fluxes using CO_2/CO correlations in Asian outflow. *J. Geophys. Res.* **2004**, *109*, D18S18. [CrossRef]
28. Keppel-Aleks, G.; Wennberg, P.O.; Schneider, T. Sources of variations in total column carbon dioxide. *Atmos. Chem. Phys.* **2011**, *11*, 3581–3593. [CrossRef]
29. Specht, D.F. A general regression neural network. *IEEE Trans. Neural Netw.* **1991**, *2*, 569–576. [CrossRef] [PubMed]
30. Cigizoglu, H.K.; Alp, M. Generalized regression neural network in modelling river sediment yield. *Adv. Eng. Softw.* **2006**, *37*, 63–68. [CrossRef]
31. Delon, C.; SerçA, D.; Boissard, C.; Dupont, R.; Dutot, A.; Laville, P.; De Rosnay, P.; Delmas, R. Soil NO emissions modelling using artificial neural network. *Tellus B: Chem. Phys. Meteorol.* **2007**, *59*, 502–513. [CrossRef]
32. Disorntetiwat, P.; Dagli, C.H. Simple Ensemble-averaging model based on Generalized Regression Neural Network in Finacial Forecasing Problems. In Proceedings of the Adaptive Systems for Signal Processing Communications, and Control Symposium, Lake Louise, AB, Canada, 1–4 October 2000; pp. 204–218.
33. Liu, D.; Lei, L.P.; Guo, L.J.; Zeng, Z.C. A Cluster of CO_2 Change Characteristics with GOSAT Observations for Viewing the Spatial Pattern of CO_2 Emission and Absorption. *Atmosphere* **2015**, *6*, 1695–1713. [CrossRef]
34. Bie, N.; Lei, L.P.; Zeng, Z.C.; Cai, B.F.; Yang, S.Y.; He, Z.H.; Wu, C.J.; Nassar, R. Regional uncertainty of GOSAT XCO_2 retrievals in China: Quantification and attribution. *Atmos. Meas. Tech. Discuss.* **2018**, *11*, 1251–1272. [CrossRef]